CHAPTER 3

Effects of Solvothermal Etching and $TiCl_4$ Treatment of TiO_2 Nanorods (TNRs) ETL on the Performance Characteristics of FTO/TNRs/$CH_3NH_3PbI_3$/Spiro-OMeTAD/Pd Solar Cells*

Contents

*Part of this work has been published as:

1. Jarwal, Deepak Kumar, et al. “Efficiency improvement of TiO_2 nanorods electron transport layer based perovskite solar cells by solvothermal etching.” *IEEE Journal of Photovoltaics* 9.6 (2019):1699-1707.

CHAPTER 3

Effects of Solvothermal Etching and $TiCl_4$ Treatment of TiO_2 Nanorods (TNRs) ETL on the Performance Characteristics of FTO/TNRs/$CH_3NH_3PbI_3$/Spiro-OMeTAD/Pd Solar Cells

3.1 Introduction

The effect of the TiO_2 nanorods (TNRs) based ETL thickness on the performance parameters of FTO/TNRs/$CH_3NH_3PbI_3$/PTAA/Pd perovskite solar cells (PSCs) has been discussed in Chapter-2. It may be mentioned that the morphology and shape of the TNRs surface play crucial roles in the performance improvement of the PSCs [135]. Thus, an attempt has been made in this chapter to improve the performance of the FTO/TNRs/$CH_3NH_3PbI_3$/Spiro-OMeTAD/Pd by solvothermal etching and $TiCl_4$ treatment of the hydrothermally grown TNRs based ETL by the low-cost hydrothermal method considered in Chapter-1 [136]. To show the robustness of the PSCs, both the fabrication and measurements have been carried out at room temperature and the high humid open-air environment with a relative humidity of ~65% or above. The top of TNRs in the ETL has been split into small nanowires and nanotubes by the solvothermal etching of the TNRs to speed-up electron transportation, enhance porosity, and increase the effective surface-to-volume ratio of the ETL [81]. The TNRs have been finally treated with $TiCl_4$ to improve the fill factor (FF) and open-circuit voltage (V_{OC}) of the hybrid PSCs under study [63]. The outline of the rest of the present chapter is as follows:

Section 3.2 contains the experimental detail for the synthesis of materials and fabrication of PSCs. The measurement of different solar parameters and their discussion

are presented in Section 3.3. Finally, the finding and observations of the present chapter are summarized in Section 3.4.

3.2 Experimental Details

This section deals with the fabrication and characterization details of the TNRs ETL based hybrid PSC solar cells on fluorine-doped tin oxide (FTO) coated glass substrates. 4-tert-butylpyridine, lithium bis (trifluoromethanesulfonyl)-imide, and Spiro-OMeTAD were purchased from Ossila (UK).

3.2.1 Preparation of Electron Transport Layer (ETL)

TiO_2 NRAs used for the ETL were grown on a cleaned FTO coated substrate through multiple steps, as demonstrated in Figure 3.1. A seed layer (~20 nm) of TiO_2 nanoparticles was first deposited on FTO coated substrate to achieve fast nucleation for the growth of isolated and uniform TNRs [137]. Then TiO_2 NRAs were grown on the seed layer by the hydrothermal method under optimized time and temperature. Solvothermal etching of TiO_2 NRAs was then performed to enhance the effective surface area of the ETL. Finally, $TiCl_4$ treatment of the NRAs was performed for removing the traps and voids in the TiO_2 NRAs. Four major steps in the fabrication of TiO_2 NRA based ETL is described below:

1) TiO_2 Seed Layer Deposition

A solution of TiO_2 nanoparticles (NPs) was prepared from TTIP by modifying the synthesis method reported in [138]-[139]. First of all, 740 µl of TTIP and 70 µl of HCl (~35 wt% concentration) are mixed in 2.5 ml ethanol separately. Diluted HCl solution was added drop by drop to the diluted solution of TTIP under magnetic stirring for 3 hours till the mixed solution was turned to opaque in color at room temperature. Finally, the prepared TiO_2 NPs solution was filtered by PVDF filter to achieve colloidal TiO_2

NPs of uniform size. The FTO coated glass substrates of 15 mm×45 mm was cleaned ultrasonically using soap solution, DI water, acetone and iso-propanol sequentially for 15 minutes each. The substrates were then dried at 100^{o}C and processed for plasma cleaning for 10 minutes. After the plasma cleaning of the FTO substrates, a seed layer (~ 20 nm thicknesses) of TiO_2 NPs was grown on the cleaned FTO substrates by spin coating of the colloidal TiO_2 NPs at 4000 rpm. The TiO_2 NPs coated FTO substrates were then annealed at 450^{o}C for 1 hour to prepare the compact layer (C-TiO_2) to block holes in the hybrid PSC.

2) TiO_2 Nanorod Grown by Hydrothermal Process

TiO_2 nanorods were grown hydrothermally on spin-coated TiO_2 seed layer (C-TiO_2) by using a Teflon lined autoclave at 170^{o}C through a modified synthesis route [137]. First of all, TTIP of ~560 µl was added to DI water, and the obtained white precipitate at the bottom of the solution was dissolved further in the solution of HCl (35 wt% concentration) and DI water (1:1 ratio). The mixed solution was put in a Teflon lined cylinder and the seed layer deposited FTO substrates (with FTO coated surface in the backside) were placed tilted in the TTIP solution of the cylinder in such a way that the TiO_2 NRA could grow on FTO coated surface in the downward direction as shown in Figure 3.1 (c). The Teflon lined cylinder was then sealed properly and kept into an autoclave, which was heated in the digital muffle furnace (Escon lab. Inst, India) at 170^o C for 3 hours. Since the length and diameter of TNRs are dependent on the growth time and temperature, the above temperature and duration were optimized for the desired length and diameter of the NRs in the present study. Then the autoclave was cooled down to room temperature for getting TiO_2 NRs of ~450 nm long in 3 hours. The glass substrate with TNRs grown on the FTO coated side was ringed in DI water, washed in ethanol and dried at 100^{o}C. Finally, the samples with TiO_2 NRs were annealed at 450^{o}C

for 1.30 hours in the air environment for preparing the ETL layer.

3) Solvothermal Etching of TiO_2 Nanorods

The FTO coated glass substrates with TiO_2 nanorods (TNRs) were processed for solvothermal etching of the TNRs [140]. The TNRs based substrates were placed in an etching solution prepared by mixing of 15 ml concentrated HCl (35 wt%) and 15 ml DI-water in a Teflon lined cylinder.

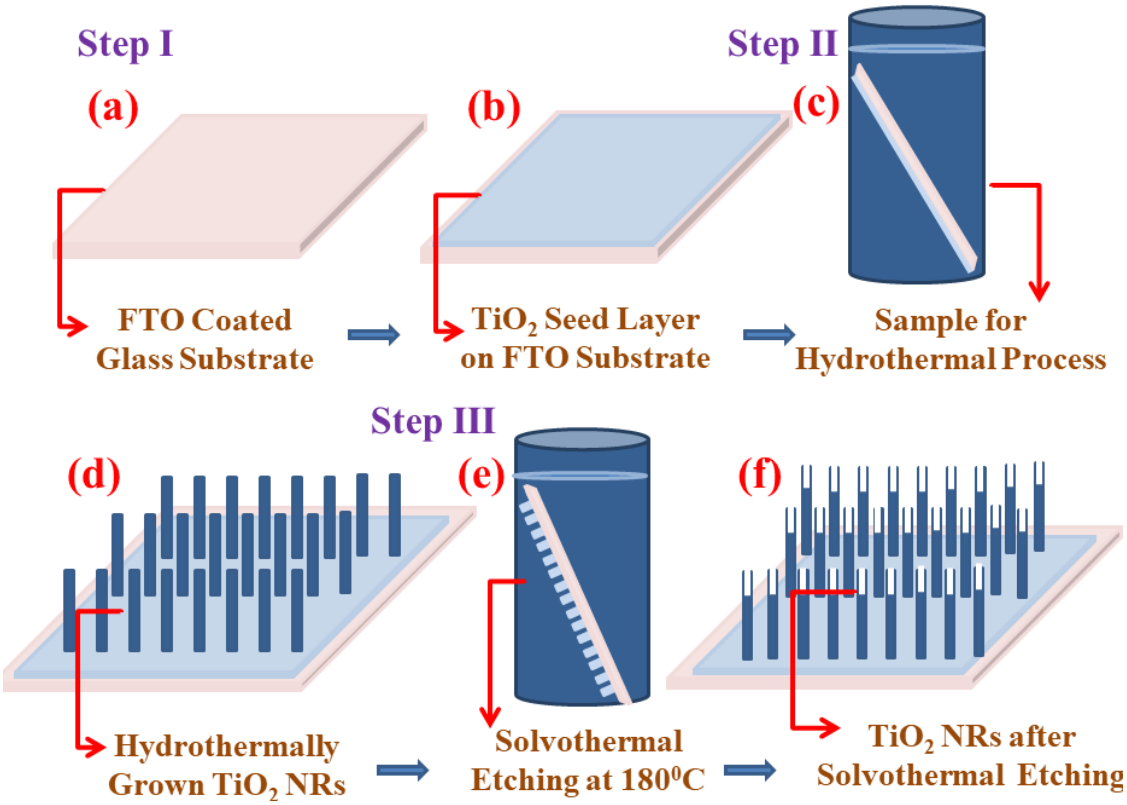

Figure 3.1: (a) FTO coated glass, (b) TiO_2 seed layer on FTO coated glass, (c) Hydrothermal Process at 170^0C in Teflon lined cylinder, (d) TNRs after hydrothermal process, (e) Solvothermal etching of TNRs at 180^0 C and (f) TiO_2 NRs after solvothermal etching.

The cylinder was placed in the autoclave, which was heated in the digital muffle furnace at a temperature of 180^o C for an optimized duration of 4-5 hours. The autoclave was then cooled down to the ambient temperature to achieve the solvothermally etched TNRs on the FTO coated glass substrates. The reaction for

solvothermal treatment is given as follows [81]:

$$TiO_2 \Leftrightarrow Ti\,(\mathrm{IV})\ \text{complex} \tag{3.1}$$

This dissolution reaction is dynamic in nature, which results in the formation of TiO_2 hollow rectangular structure (nanotubes) with filaments like appearance at the top with small nanoparticles.

4) $TiCl_4$ Treatment to Etched TiO_2 Nanorod

The substrates containing solvothermally etched TNRs were processed for $TiCl_4$ treatment to remove trap states and voids present in the TNRs based ETL. For $TiCl_4$ treatment, the substrate was immersed in a 40 mM aqueous solution of $TiCl_4$ for 30 minutes at the optimized temperature of 70^{o}C, followed by washing with DI water to remove excess salt, and annealed at 500°C for 1 hour [81].

3.2.2 Solar Cell Fabrication

The hybrid perovskite layer was obtained by two-stage spin-coating of organic and inorganic precursor solutions prepared by dissolving 462 mg of PbI_2 in 1 ml of DMF solvent and 10 mg of methylammonium iodide (CH_3NH_3I) in 1 ml isopropanol solvent, respectively. The PbI_2 solution was heated at 70°C with stirring for 1 hour and then used to deposit on the TNRs by spin coating at 3000 rpm for 40 seconds. The sample was then heated on the hot plate at 70^{o}C for 10 minutes. The CH_3NH_3I solution was then deposited on the PbI_2 layer as a second precursor at 3000 rpm by spin coating to complete the perovskite film. Toluene was used as an anti-solvent during the spin coating of CH_3NH_3I for improving the surface morphology of the perovskite film. Toluene was also used to improve the conductivity of the hybrid perovskite film by removing the voids and residues in methylammonium and halide ions [141]. The substrate containing the hybrid perovskite film was heated at 100 ^{o}C for 30 minutes for

improving its crystalline structure. Since perovskite behaves as conductive material, a thick (~100 nm) capping layer or hole transport layer (HTL) of p-type Spiro-OMeTAD (i.e. hole transport material (HTM)) was grown on the perovskite layer by spin coating method to avoid the possibility of short-circuiting between perovskite layer and top electrode of the solar cell. The HTM solution was prepared by mixing of 17.5 µl lithium bis (trifluoromethanesulfonyl)-imide [Li-TFSI] (520 mg/ml in acetonitrile), 28.8 µl of tert-butylpyridine (4-TBP), and 72.3 mg of Spiro-OMeTAD in 1 ml of chlorobenzene. The HTM solution of ~40 µl was dispersed onto perovskite and then used for spin coating at 2000 rpm for 30 seconds to achieve a ~100 nm capping layer. The capping layer also helps in improving the performance by making a balance between the shunt resistance and series resistance of the solar cell [40].

To complete the fabrication of the PSC under study, a ~ 60 nm film of palladium was deposited for top electrode by thermal evaporation (FL400, Hind High Vacuum Ltd, India with in-built thickness monitor: SQM-160, INFICON) at a vacuum of $\sim 2\times 10^{-6}$ mbar. The complete fabrication steps of three types of PSCs- Device A: PSC with simple TNRs based ETL without $TiCl_4$ and solvothermal etching; Device B: PSC with only $TiCl_4$ treated TNRs based ETL but no etching; and Device C: PSC using TNRs ETL treated with both the $TiCl_4$ and solvothermal; is illustrated in Figure 3.2. The block diagram of as-fabricated PSCs after solvothermal etching is shown in Figure 3.3 (a). The energy level of various material layers in the PSC structure is analyzed through the energy band diagram shown in Figure 3.3 (b). Note that electrons and holes after separation of the photo-generated electron-hole pairs travel in opposite directions with the help of ETL and HTL.

3.2.3 Material and Device Characterization

The crystalline structure of the prepared TNRs grown on FTO coated glass was characterized by X-ray diffractometer (XRD, Miniflex, Rigaku, Japan) by using Cu-Ka at a wavelength of λ = 1.5406Å for an operating voltage of 45 kV and current of 40 mA. The structure and crystallinity of TNRs are analyzed using transmission electron microscopy (TEM) (FEI G2 T20 STWIN). The elemental composition of the sample was evaluated by energy dispersion spectroscopy (EDS) (EDAX Inc.), and the surface morphology of the sample was recorded by high-resolution scanning emission microscopy (HRSEM) (Nova Nano SEM 450, FEI, USA). The roughness of the TiO_2 layer and perovskite layer is analyzed by atomic force microscopy (AFM) (NTEGRA Prima, NT-MDT Service & Logistics Ltd.). The transmittance and absorbance spectra were obtained from the dual-beam UV-Vis

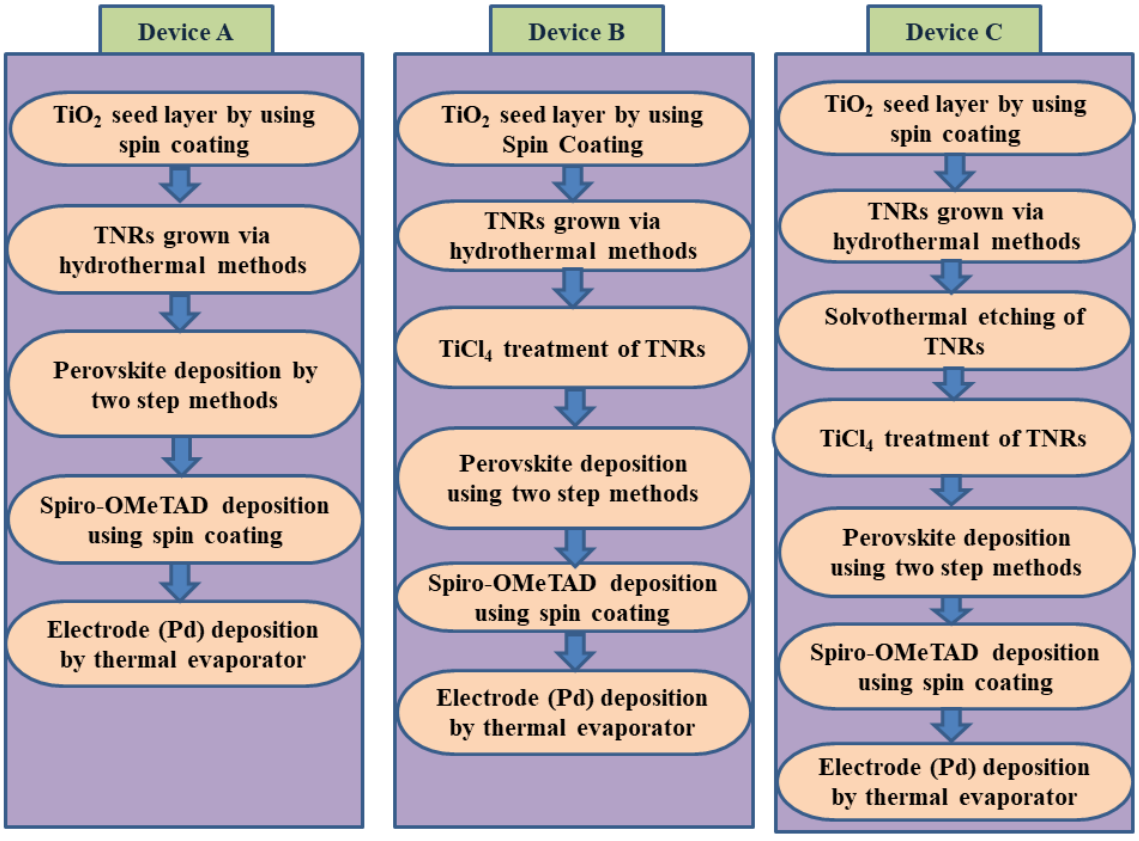

Figure 3.2: Fabrication steps used for device A, B and C.

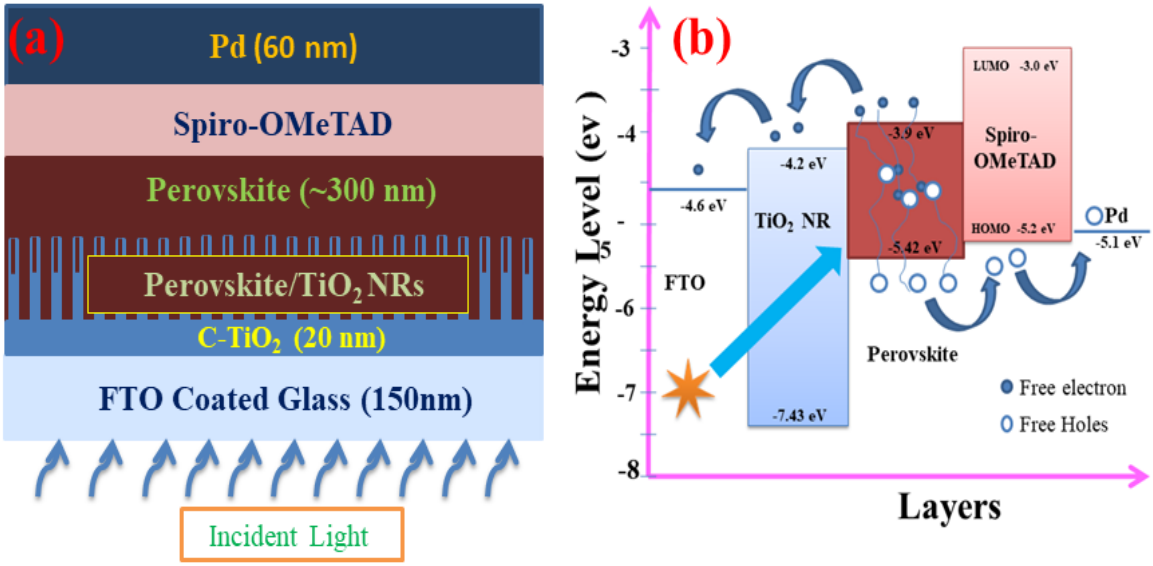

Figure 3.3: (a) The device structure of PSC after solvothermal etching of TiO_2 NRs and (b) Schematic representation of the energy band diagram of PSC.

spectrophotometer (Jesco, V-750, Japan). The photoluminescence measurement is performed using spectrometer (FLS 980 from Edinburgh Instruments, UK). The electrical measurement including current-voltage (*IV*) and impedance of the solar cells was performed using probe station attached to the semiconductor parameter analyzer (B1500A, Keysight). Solar light spectrum of 100 mW/cm^2 and 1.5 AM G is obtained from solar simulator (PET corp., USA). The external quantum efficiency (EQE) was measured from the experimental setup of monochromator (SP2150i, Princeton Instruments, USA) connected with light source (Princeton Instruments) and digital multimeter (DMM, 34410A, Agilent). The power of the incident light and output current of the device at different wavelength was measured using power meter (PM100D, Thorlabs) and DMM, respectively, connected through LabVIEW software.

3.3 Results and Discussion

The measured solar characteristics and parameters are presented in this section. Further discussion on the solar cell characteristics is also listed in this section.

3.3.1 Thin Film Characterization

X-ray diffraction analysis was used to investigate the crystallinity and phase of the TiO_2 film. The diffractogram of the TNRs is shown in Figure 3.4 (a) from 5 degrees to 80 degree for a step of 0.0200 degree. It is observed that grown TNRs have both anatase and rutile phases. The experimental XRD pattern is well-indexed to the tetragonal rutile phase (JCPDS No. 21-1276). Stronger diffraction peaks at 26.90 degree, 36.49 degree and 54.89 degree over two minor peaks (at 63.15 degree and 70.17 degree) of the anatase phase confirm rutile as the majority phase in the TNRs. Two spurious diffraction peaks at 42.84 degree and 71.08 degree are also observed. The XRD pattern of the TNRs before and after the solvothermal treatment exhibit the same diffraction peaks as shown by the Wan et al.[81]. This clearly rules out any possibility of phase transformation or any new phase formation during the solvothermal etching process. The elemental composition analysis through energy dispersive spectroscopy (EDS) is shown in Figure 3.4 (b).

The surface morphology and structure of individual TNR obtained by TEM analysis is shown in Figure 3.5. The bright field images in Figure 3.5 (a) and (c) show the diameter of TNRs before and after solvothermal etching of TNRs. The selected area electron diffraction pattern (SAED) in Figure 3.5 (b) and (d) confirm that TNRs are of single crystalline rutile phase. Figure 3.5 (c) also shows small TiO_2 nanoparticles with TNRs which could have formed due to dissolution and reprecipitation during solvothermal etching treatment.

The scanning electron microscopy (SEM) images of TiO_2 NRs are shown in Figure 3.6. The SEM images of the TNRs before the solvothermal etching in Figure 3.6 (a) and (b) show that TNRs are uniformly distributed over the FTO substrate having average length around ~ 450 nm and an average diameter of ~150 nm. The length and diameter are also

measured from the cross-sectional HRSEM shown in the inset of Figure 3.6 (b). The surface morphology and density of TNRs can be optimized by changing the concentration of precursor (TTIP) in the solution. The length and diameter of TNRs are dependent on the temperature and time of the hydrothermal process. It is also observed that there is a significant space between any two TNRs, which can be explored to place the perovskite material

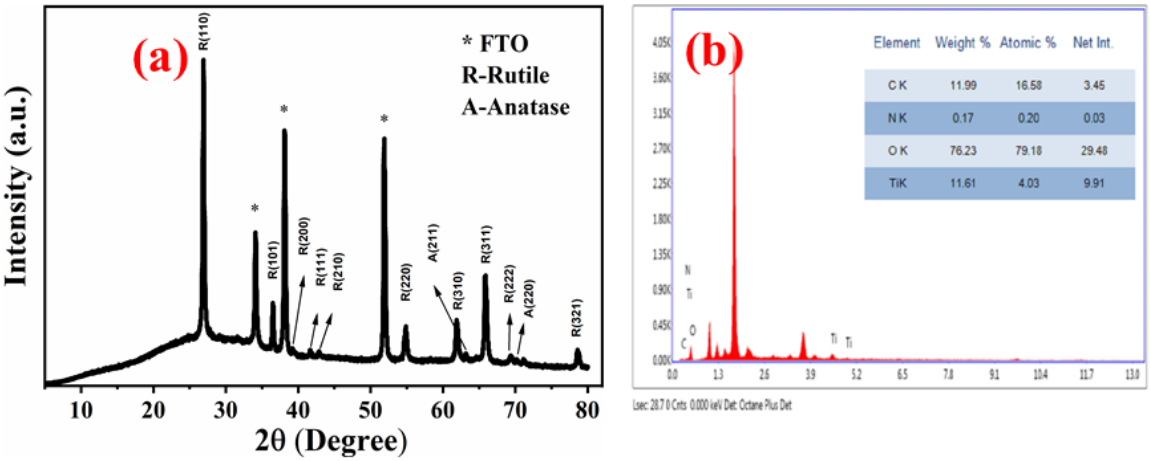

Figure 3.4: (a) XRD analysis of TiO_2 NRs annealed at 450^0 C. (b) Energy dispersive spectroscopy (EDS) and elemental composition of TNRs.

of the PSC under study. The solvothermal etching improves the net surface area of the TNRs by splitting their top surfaces into small nanowires and hollow rectangular structures in the form of nanotubes ~70 nm diameter and ~ 100 nm depth, as shown in Figure 3.6 (c) and (d). The inner diameter and depth of the rectangular hollow voids can be increased by enhancing the etching time and temperature. The surface morphology and grain of the perovskite layer deposited on TiO_2 NRs (TNRs) at room temperature and 65% relative humidity are shown in Figure 3.6 (e) and (f). The surface roughness and grain boundaries of the TNRs layer before and after the solvothermal treatment are analyzed from AFM images shown in Figure 3.7 (a)-(b) and 3.7 (c)-(d), respectively.

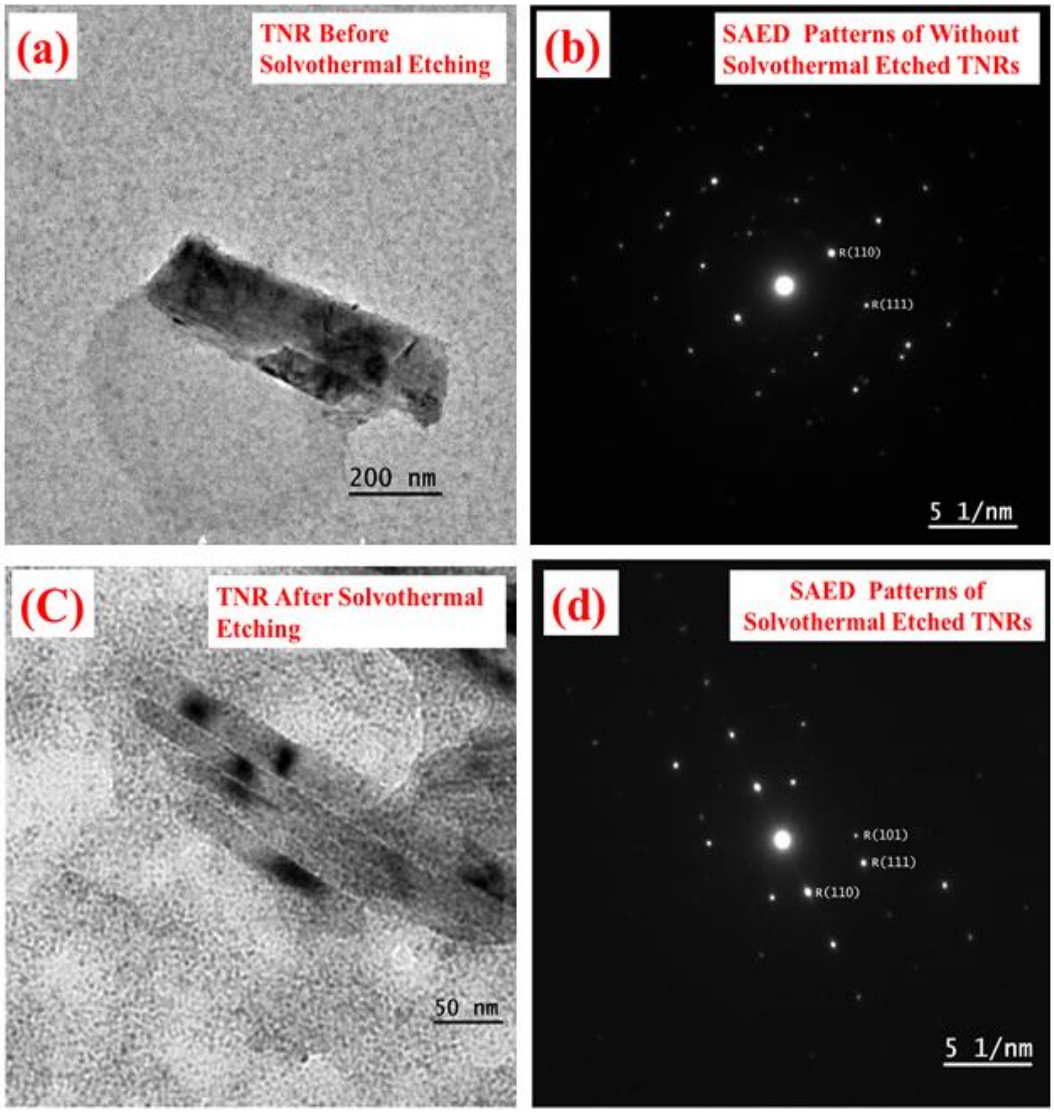

Figure 3.5: (a) and (c) are the TEM images of pristine rutile TNRs and TNRs after solvothermal etching respectively. Figure (b) and (d) are the selected area electron diffraction patterns corresponds to Figure (a) and (b) respectively.

The AFM images of the perovskite layer deposited on the solvothermally etched TNRs layer have been shown in Figure 3.7 (e)-(f). The root-mean-square (RMS) surface roughness of TNRs before solvothermal etching, TNRs after solvothermal etching, and perovskite layer on TNRs are measured as ~100 nm, ~112 nm, and ~56 nm, respectively. The roughness profile confirms that the TNRs layer after solvothermal etching has larger surface roughness than that of the TNRs layer without etching. In other words, the overall active surface area of the device is increased by solvothermal

etching, which can be explored for enhancing the efficiency of PSC. The AFM results are found to be agreed with the SEM results shown in Figure 3.6.

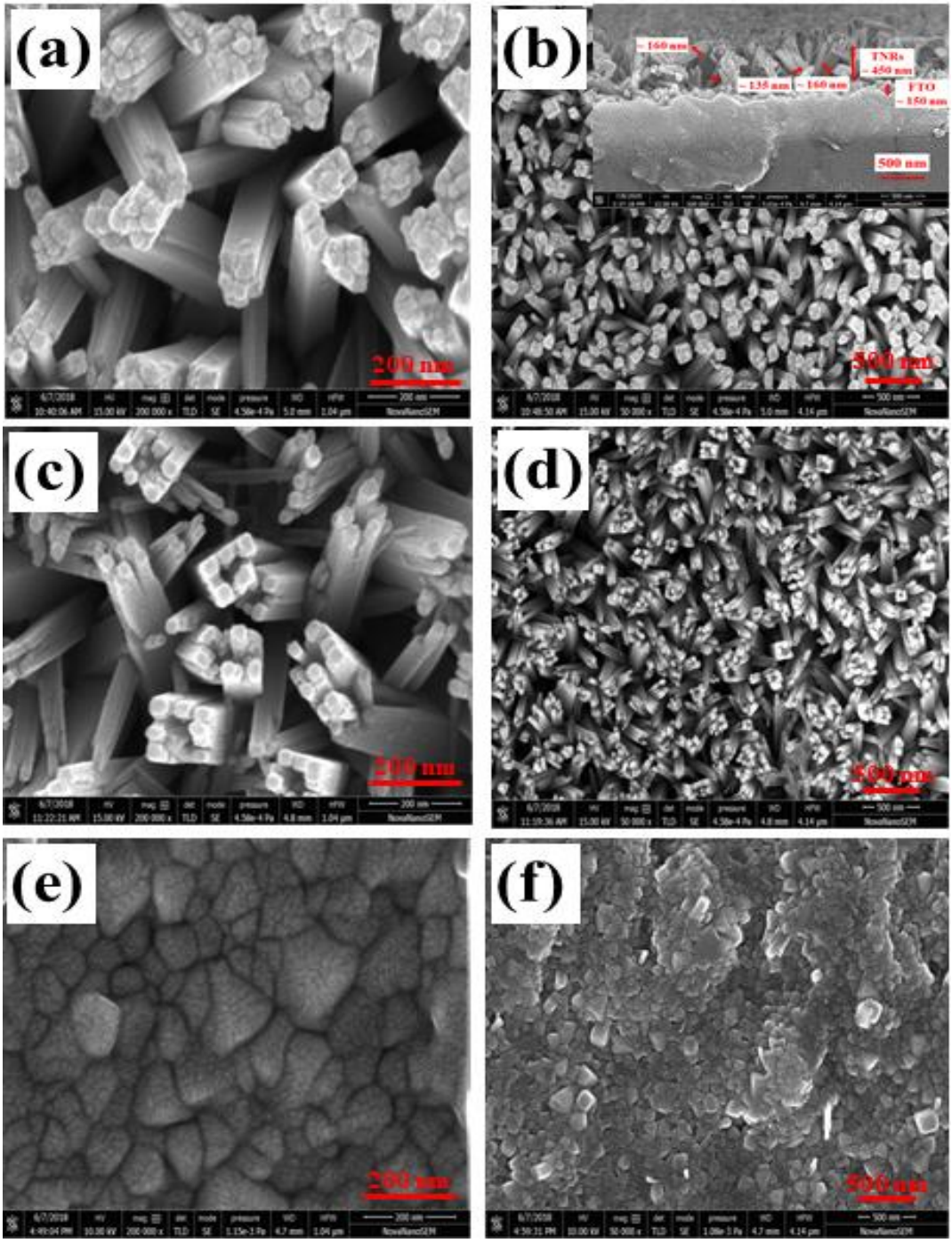

Figure 3.6: Top view SEM image of TNRs annealed at 450^0 C in ambient environment before solvothermal etching: (a) 200 nm scale, (b) 500 nm scale (Inset of Figure 3.6 (b) shows the cross-sectional image of TNRs at 500 nm scale); after solvothermal etching: (c) 200 nm scale, (d) 500 nm scale. Top SEM image of perovskite thin film deposited on solvothermal etched TNRs (e) 200 nm scale and (f) 500 nm scale.

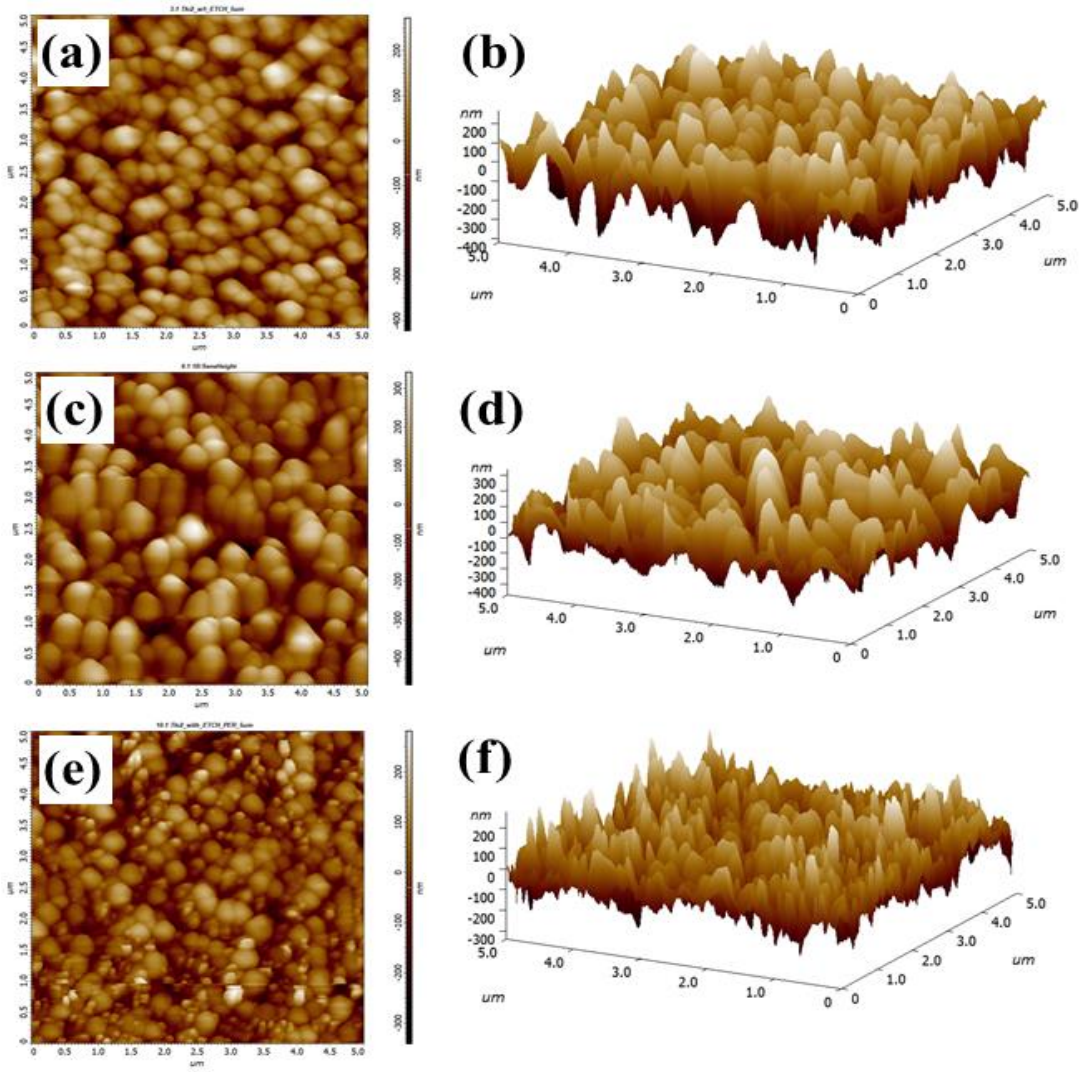

Figure 3.7: AFM image of TNRs without solvothermal etching (a) 2D and (b) 3D. AFM image of TNRs with solvothermal etching (c) 2D and (d) 3D. AFM image of perovskite film deposited on etched TNRs (e) 2D and (f) 3D.

The transmittance (T) spectra of TNRs without solvothermal etching and with solvothermal etching are shown in Figure 3.8 (a). Note that absorption in TNRs can be written as

A=log (1/T) [143]. Similar transmittance spectra pattern confirms that no change in phase of the TNRs is introduced by the solvothermal etching process except change in their effective surface area as also supported TEM image and SAED pattern of TNR (as shown in Figure 3.5). Also, the TNRs along with nanoparticles (as confirmed by TEM image) may

further enhance the surface to volume ratio of the TNRs layer, which enhances the absorbance. A step-change in the transmittance spectra observed at ~405 nm due to an abrupt reduction in absorption near the optical bandgap edge of TiO_2. The value of optical band gap can be calculated from the tauc relationship [143]:

$$\alpha h\upsilon = \mathrm{A}(h\upsilon - E_g)^m \tag{3.2}$$

Where $$\alpha = 2.33\log(T/d) \tag{3.3}$$

is the absorbance coefficient, d is the sample thickness, and $h\nu$ = 1240/(incident light (nm)) is the photon energy. The estimated bandgap of the TiO_2 is ~3.2 eV, which has been derived from the plot of $(\alpha h\nu)^{1/2}$ versus ($h\nu$). For wavelengths below 400 nm, the absorption in TNRs (TiO_2 nanorods) after etching is more than the TNRs without etching, which may be attributed to the partial dissolution of TNRs in solvothermal etching as also noticed in the SEM images. It is observed that the perovskite layer on solvothermal etched TNRs has more absorbance compare to the perovskite layer on the other two kinds of TNRs layers, as shown in Figure 3.8 (b).

The charge transport and traps in different ETL films of the solar cell structure are studied using the electrical as well as optical measurements shown in Figure 3.9. The *I-V* characteristics of three Ag/TNRs based junction diodes made of three different types of TNRs (Device 1: TNRs, Device 2: TNRs/$TiCl_4$ treated, and Device 3: TNRs/Etched/$TiCl_4$ treated) are compared in Figure 3.9 (a). The improved diode current in Device 2 and Device 3 over Device 1 is clearly observed due to a reduction in traps in the modified TNRs treated with $TiCl_4$. The space charge limited current (SCLC) region of the *IV* characteristics are shown in the inset of Figure 3.9 (a). It can be noted from the SCLC region that the carrier mobility is increased significantly with the solvothermal etching followed by $TiCl_4$ treatment. The effect of modified TNRs on the

optically generated charge carriers of PSCs is also investigated in terms of the PL quenching shown in Figure 3.9 (b). The subsequent decrease in PL intensity for Device B and Device C confirms the enhancement in the photoabsorption and photocurrent in the PSCs under study. The enhanced absorption also agrees with the results shown in Figure 3.8 (b). Finally, the impedance characteristics of all the three

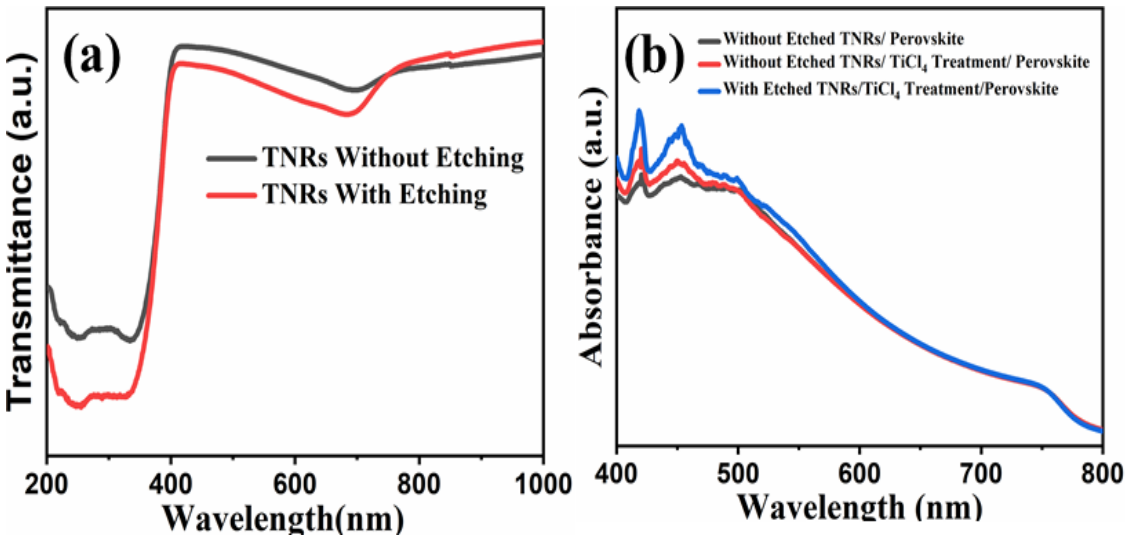

Figure 3.8: (a) Transmittance of TiO_2 NRs before and after solvothermal etching. (b) UV-VIS absorbance spectrum of perovskite film deposited on TiO_2 nanorods without $TiCl_4$ treatment, TiO_2 nanorods with $TiCl_4$ treatment before and after solvothermal etching.

solar cell structures measured at an applied voltage of 1 V in the frequency range of 1 kHz to 1 MHz are plotted in the inset of Figure 3.9 (b). It is found that the impedance is reduced due to $TiCl_4$ treatment of the TNRs based ETL.

3.3.2 Solar Cell Characterization

The photocurrent density (J_{ph}) vs. voltage (V) characteristic was recorded by a semiconductor parameter analyzer under the illumination of the solar spectrum through a circular mask having an area equal to the cell area of 0.0314 cm^2. The solar cell parameters such as V_{OC}, J_{SC}, FF, and PCE are obtained from the J_{ph}-V characteristic shown in Figure 3.10 (a). The solar cell parameters for different device structures are

summarized in Table 3.1. The performance of the following three types of fabricated PSC is investigated in this article. The average PCE of 11.46%, V_{OC} of 0.97 V, J_{SC} of 20.75 mA/cm^{2,} and FF of 0.55 are obtained for "Device A". The performance parameters are observed to be improved by $TiCl_4$ treatment of the ETL since the PCE of 12.90%, V_{OC} of 1.01 V, J_{SC} of 22.19 mA/cm^2, and FF of 0.57 are measured for "Device B". The performance improvement in "Device B" over "Device A" is attributed to the enhancement of carrier lifetime and diffusion length achieved by removing the traps and voids from TNRs by the $TiCl_4$ treatment of "Device B". Note that traps and voids in TNRs enhance the recombination of charge carriers and limit the diffusion length of carriers. "Device C" fabricated by using TNRs ETL with solvothermal etching followed by $TiCl_4$ treatment has an average PCE of 14.78%, FF of 62%, V_{OC} of 1.05 V, and J_{SC} of 22.31 mA/cm^{2,} which are the best among all the three types of PSCs (i.e., A, B, and C) considered in this study.

It is important to mention that the cell parameters discussed above are directly affected by the values of the shunt resistance (R_{Sh}), series resistance (R_S), and other losses in the devices [144]. The decrease in series resistance and increase in shunt resistance enhance the value of FF, which, in turn, results in higher PCE and optimizes the output power close to the theoretical maximum value [144]. The results confirm that the solvothermal etching process along with $TiCl_4$ treatment can be explored for improving the performance of the TNRs ETL based hybrid PSCs by reducing the surface traps and defects in TNRs by the $TiCl_4$ treatment and enhancing the effective light absorption area by the solvothermal etching process. The highest PCE of 15.16% is achieved for the champion Device-C along with FF of 0.64, J_{SC} of 22.64 mA/cm^{2,} and V_{OC} of 1.04, which are possibly the best under open-air measurements. The power conversion efficiency of $MAPbI_3$ and different type of TiO_2 ETL based PSCs are compared in

Table 3.2. Clearly, the use of modified TNRs based ETL in our proposed device shows promising power conversion efficiency under high humid and open atmosphere. The efficiency is believed to be enhanced further if the fabrication and measurements are performed in a controlled environment which is not available in our laboratory. We will consider the external quantum efficiency (EQE) of the devices A, B, and C compared in Figure 3.10 (b). The EQE is computed by using the following relation [145]:

$$EQE = 1240 \times \left(\frac{R}{\lambda}\right) \times 100\% \tag{3.4}$$

Where 'R' is the photoresponsivity and λ in the wavelength of the incident light. Figure 3.10 (b) shows the highest value of EQE in Device C, which again confirms its superior performance over the other two devices.

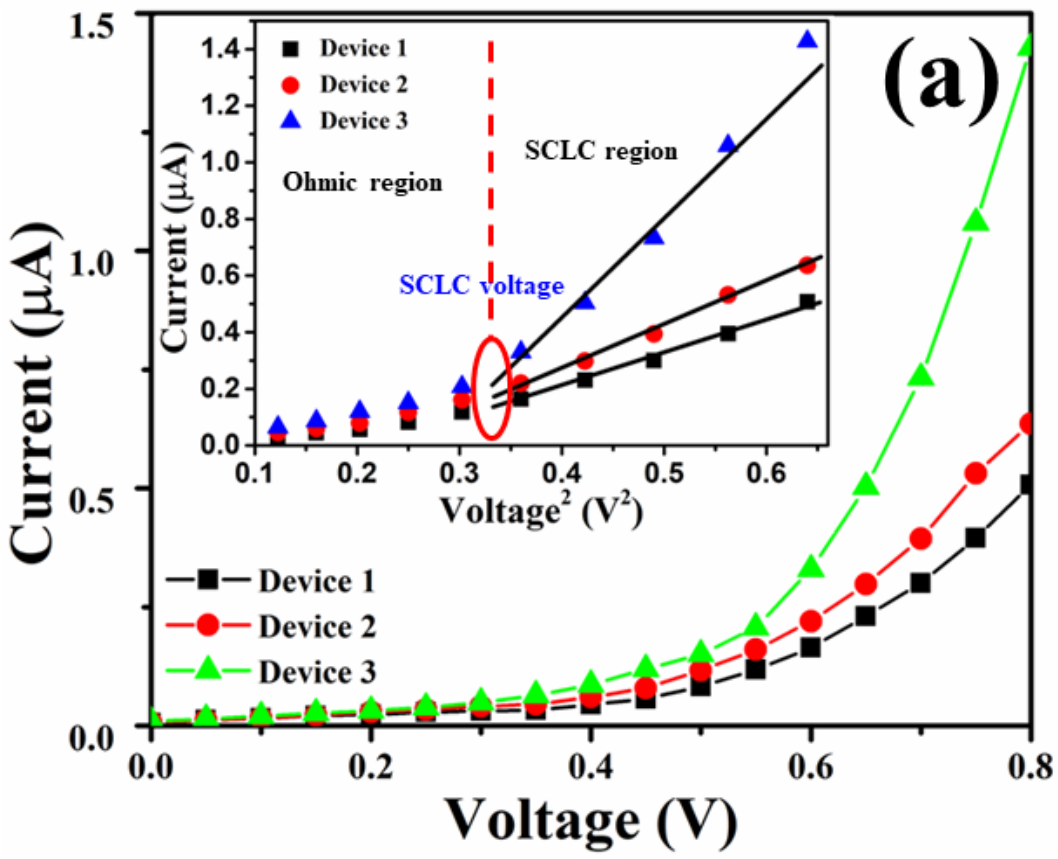

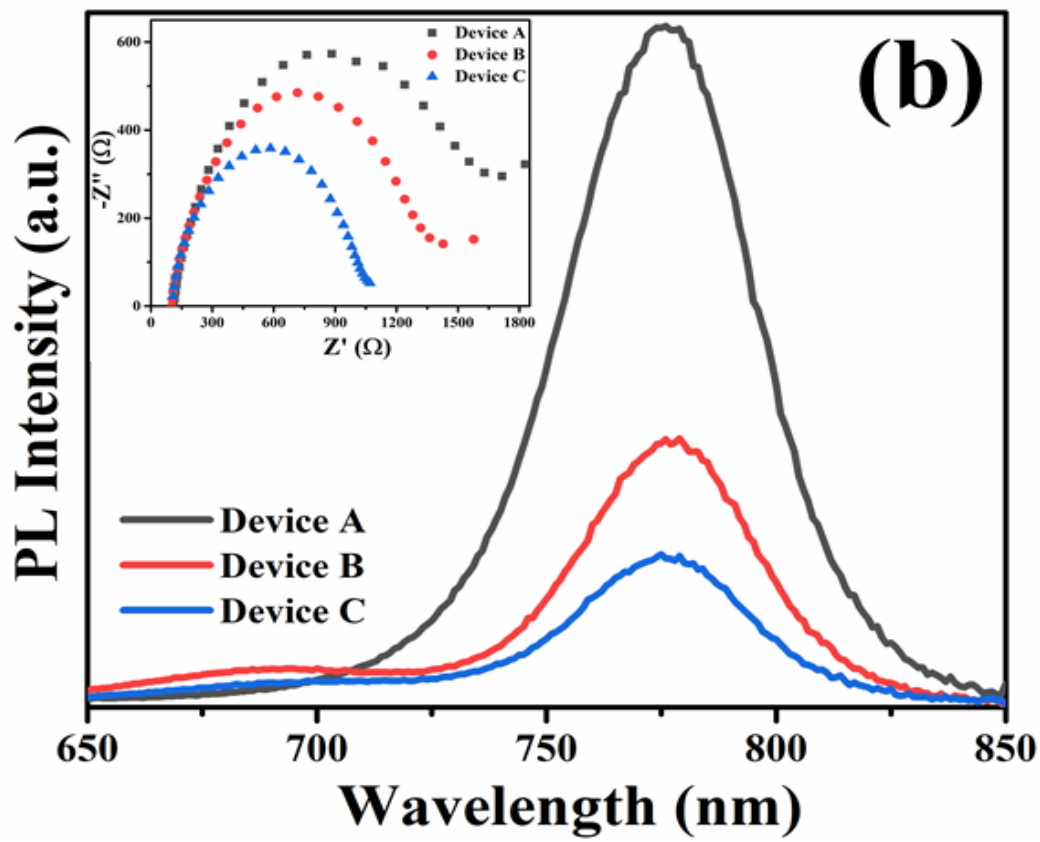

Figure 3.9: (a) *I-V* characteristics of the junction diode made of modified TNRs. Inset of (a) shows SCLC region in all the diode. (b) Emission characteristics in three solar cell structures. of TiO_2 NRs before and after solvothermal etching. Inset of (b) shows impedance characteristics of three solar cells.

Table 3.1: Device Comparison based on TiO_2 NRs ETL

Device Parameter / ETL		J_{sc} (mA/cm^2)	V_{oc} (V)	FF	PCE (%)
TNRs (Device A)	Average	20.75 ± 02.25	0.97 ± 0.04	0.55 ± 0.05	11.46 ± 0.65
	Champion	20.18	0.964	0.61	12.03
TNRs/$TiCl_4$ treated (Device B)	Average	22.19 ± 01.5	1.01 ± 0.04	0.57±0.04	12.90 ± 1.36
	Champion	22.18	1.07	0.61	14.55
TNRs/Etched/$TiCl_4$ treated (Device C)	Average	22.31 ± 0.30	1.05 ± 0.04	0.62 ±0.02	14.78 ± 0.45
	Champion	22.64	1.04	0.64	15.16

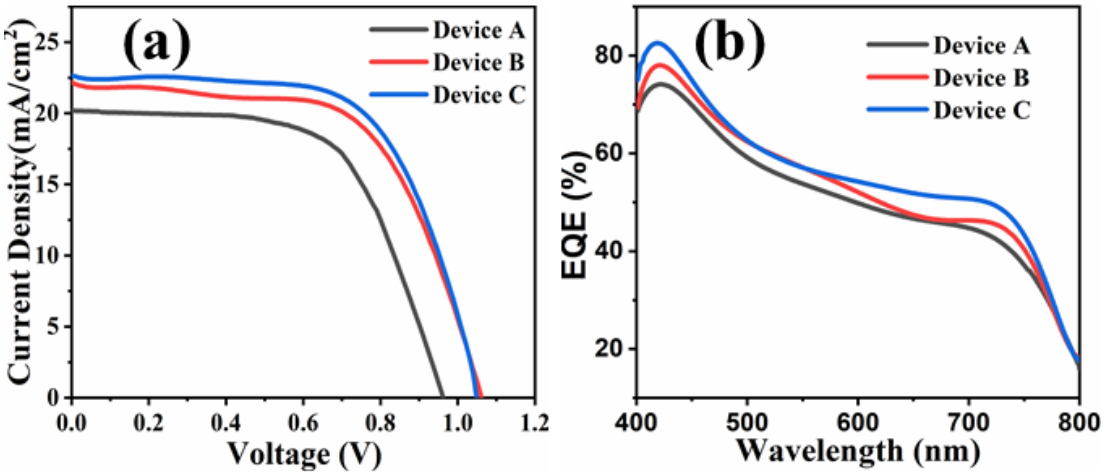

Figure 3.10: (a) Jp_h-V characteristics of device A, B & C; (b) Comparison of EQE of device A, B & C.

TABLE 3.2: POWER CONVERSION EFFICIENCY OF TiO_2 ETL BASED PSCS.

ETL	PCE (%)	Ref.
TiO_2 nanorods	9.4	[146]
TiO_2 nanowire	11.7	[75]
Bare TiO_2 NR $TiCl_4$-treated TiO_2 NR 4.8 nm TiO_2 nanoparticle on TNRs $TiCl_4$-treated mesoporous- TiO_2	5.03 7.98 13.45 9.58	[147]
TiO_2 NP film (0.4 vol %) rGO/mesoporous- TiO_2	11.5 13.5	[148]
TiO_2 nanoparticles TiO_2 nanotubes TiO_2 nanotube/TiO_2 nanoparticle	6.56 7.63 9.16	[149]
TiO_2 mesoporous	12.62	[150]
Rutile TiO_2 nanorod	16.11	[151]
Compact- TiO_2 Compact- TiO_2 / mesoporous- TiO_2	11.85 14.76	[152]
TiO_2 (Compact + mesoporous) 0.5 mol% Al TiO_2	11.49 14.05	[153]
TNRs/ TNRs Etching/$TiCl_4$ treatment	15.16	This Work

3.4 Conclusion

The performance improvement in hybrid PSCs by solvothermal etching and $TiCl_4$ treatment of TNRs based ETL grown on the FTO coated glass substrates have been analyzed in this chapter. The performance parameters of three types of PSCs using hydrothermally synthesized TNRs based ETLs without etching and $TiCl_4$ treatment (Device A); with only $TiCl_4$ treatment but no etching of TNRs (Device B); and TNRs with solvothermal etching followed by $TiCl_4$ treatment (Device C) are compared. The PCE, V_{OC}, J_{SC} and FF are measured as 11.46%, 0.97 V, 20.75 mA/cm^2 and 0.55 for "Device A"; 12.90%, 1.01 V, 22.19 mA/cm^2, and 0.57 for "Device B"; and, 14.78 %, 1.05 V, 22.31 mA/cm^2 and 0.62 for and "Device C". The EQE is also found to be the best for "Device C" among the three devices. The improvement in the performance parameters of "Device C" is attributed to the enhancement of recombination lifetime of carriers due to the reduction of traps and voids in the TNRs by $TiCl_4$ treatment as well as to the enhancement of the effective surface area of the TNRs by solvothermal etching.